Fibers and Polymers 2018, Vol.19, No.12, 2548-2563
DOI 10.1007/s12221-018-8306-9

ISSN 1229-9197 (print version)
ISSN 1875-0052 (electronic version)

Production of Metal Oxide Containing Antibacterial Coated Textile Material and Investigation of the Mechanism of Action

Gorkem Gedik[1]*, Aysun Aksit[1], Birol Engin[2], and Ufuk Paksu[2]

[1]*Textile Engineering Department, Dokuz Eylul University, Izmir 35390, Turkey*
[2]*Physics Department, Dokuz Eylul University, Izmir 35390, Turkey*

(Received April 18, 2018; Revised August 8, 2018; Accepted September 11, 2018)

Abstract: The main aim of this study was to produce PVC coated textile based antibacterial textile material and to investigate the antibacterial mechanism with detailed analyzes. Metal oxide (calcium oxide, zinc oxide, magnesium oxide) powders were used to provide antibacterial functionality to coated materials. Metal oxide concentrations were varied between 5-35 %. Antibacterial tests were performed according to ISO 22196-2011 standard. Antibacterial efficiency of the samples was tested for each metal oxide type and concentration with *L. innocua* species. The antibacterial mechanism was investigated with ESR technique, fluorescent microscobe and microplate reader using DCFH-DA probe, UV-vis spectrometer using fluorescein probe. The results indicated that the antibacterial effect of used metal oxides was strongly arisen from radical oxygen species. The morphology of coatings was investigated with SEM and the distribution of metal oxide particles on the surface was examined with EDX analysis and EDX mapping. The changes on the molecular basis of the coating due to the metal oxide addition was analyzed with FT-IR spectroscopy. High antibacterial efficiencies (up to 100 %) were detected. It is suggested that the non-toxic metal oxides can be used as an effective and economically feasible alternative to conventional antibacterial additives for industrial applications such as conveyor belts.

Keywords: Metal oxide, Antibacterial, Conveyor belt, ESR, Oxygen radical

Introduction

Antibacterial property of a textile might be a necessity rather than an option for some industrial areas. For instance, conveyor belts play an important role in linking and transportation of raw materials, mid-products and final products at a food producing facility [1]. Since conveyor belts are in direct contact with food materials, there should be no tolerance for bacterial growth on the belt due to the health concerns. Remarkable ratios of food-borne diseases are linked to poor hygiene conditions and insufficient cleaning procedures of the equipments. Cross contamination, which is the transfer of pathogens from infected goods to uninfected, is one of the most important points to pay attention to prevent the spread of pathogen bacteria [2]. Conveyor belts are endless systems, therefore, a bacterial contamination on a point of a belt could affect the whole production. From this point of view, food carrying conveyor belts could be gained antibacterial properties to eliminate cross contamination risks during transportation of the food materials. Since those are in direct contact with food materials, the antibacterial agents should be chosen form a very narrow list. Metal oxides, such as zinc oxide, magnesium oxide and calcium oxide are very suitable options for an antibacterial addition for food conveyor belts due to non-toxic properties [3]. Besides, opposite to organic antibacterials, metal oxides are durable to hard process conditions and maintain their antibacterial properties for a long time period [4].

*Corresponding author: gorkemgedik@live.com

Though the antibacterial activity of nano and bulk metal oxide powders has been issued by several researches, the mechanism of action is still controversial. Proposed mechanisms mainly include the damage of cell associated with metal oxide particle morphology [5-7], release of metal ions [5,8,9] and radical oxygen species (ROS) formation due to the catalytic reactions of metal oxides [5-26]. Despite those different perspectives on the antibacterial mechanism of metal oxides, recent studies generally concentrated on antibacterial action via radical oxygen species. Sawai [27] investigated the antibacterial effect of ten times higher Zn^{+2} concentration than released to aqueous solution from ZnO and reported that no antibacterial activity was observed. On the other hand, zinc oxide was found to be antibacterial. From this results, antibacterial activity of zinc oxide was validated and it is comprehensible to consider zinc ions first suspect for the antibacterial activity of ZnO. Moreover, Sawai *et al.* reported no antibacterial activity for the supernatant of zinc oxide powder slurry. This experiment eliminated the role of zinc ions on antibacterial action. They also remarked that growth inhibitory effect arises from the zinc oxide surface. They stated that, though zinc ions have a destructive effect on bacteria's vital metabolism activities, in case of zinc oxide, the low solubility in the aqueous media limits the antibacterial action of rhe Zn^{2+} ions and the antibacterial activity arises from oxygen radicals [11]. These results were in parallel line with the findings of Prasanna and Vijayaraghavan [20], Xu *et al.* [19] and Raghupati *et al.* [28] who pointed out that free zinc ions have negligible influence on antibacterial activity. Sawai *et al.* [29] also underlined that antibacterial activity of magnesium oxide was related

with oxygen radicals instead of Mg^{2+} ions. At the same study, the influence of high pH value on antibacterial activity caused by calcium oxide presence was investigated. They reported lower antibacterial activity for sodium hydroxide solutions which have higher pH value than calcium oxide suspension. This result indicated that antibacterial activity of calcium oxide can not only be explained with high pH values. Antibacterial effect of MgO and CaO was arised from oxygen radicals [27]. Roy *et al.* [30] also explained the antibacterial activity of CaO with ROS production.

One of the most important points to comprehend the catalytic reactions of metal oxides is to figure out the reaction pathways between the substrate and the metal oxide. The reaction might occur via direct electron transfer [31], photocatalytic reactions [32], OH layer on the alkali earth metal oxide surfaces [33] and surface defects (especially oxygen vacancies) [19,20].

Radicals are chemicals or materials which have one or more unpaired electrons. Radical oxygen species such as superoxide, hydroxyl, singlet oxygen and hydrogen peroxide are free radicals and very strong oxidants which are able to damage vital methabolism of living cells. ESR is very useful technique for radical researches. The basic principle of ESR is similar to nuclear magnetic resonance; however, electron spins are excited in ESR, instead of atomic nuclei [34]. Since the ROS are very short-lived species, spin-trapping techniques are carried out to work with ROS in ESR. When unstable radicals react with spin trap chemicals, they are converted to stable radicals which have sufficient life time to be monitored on ESR [35,36].

Another way to work with ROS is to use chemical probs which form stable compounds that are detectible with instrumental methods such as fluorescent microscope, flow cytometry, UV-vis spectroscopy, microplate reader and so on. DCFH-DA (dichlorofluorescein diacetate) probe which is applied to detect intercellular oxidative stress is an instance [37,38]. DCFH-DA is a non-selective oxygen radical probe which means it can react with all kind of oxygen radical species and provide information about total oxygen radical amount [37,38]. DCFH-DA is not fluorescent and do not react with ROS in the acetate form. Once it penetrates into the cell, intercellular esterases convert DCFH-DA to $DCFH_2$ form which is not fluorescent, on the other hand able to react with ROS. Also, $DCFH_2$ is not cell-membrane permeable so this molecule cannot leak out of the cell. If $DCFH_2$ reacts with oxygen radicals inside the cell, it is transformed to DCF molecule which is highly fluorescent and detectible with instrumental methods noticed above [37-39].

ROS presence can also be monitored via the fading of fluorescein due to the decomposition of this strong fluorescent chemical as a result of redox reactions. Hua *et al.* [40] investigated the decomposition of fluorescein depending of the catalytic effect of silicon nanowires modified with silver, by UV-vis spectrometer. Bardhan *et al.* [41] detected the decomposition of fluorescein due to the photocatalytic effect of zinc oxide nano powders by fluorimeter and UV-vis spectrometer.

For an effective antibacterial usage of metal oxides, double layered coating construction was carried out. By this way, it was possible to load high concentration of metal oxide powder into the polymer paste. Various concentrations of metal oxides were applied to detect optimum concentration. Metal oxides step forward as antibacterial additive for textile coating at this study since they are cheap, safe for health and environment, compatible with PVC, suitable for food carrying conveyor systems and for long term use.

The antibacterial activity of nano and bulk metal oxide powders has been investigated in the literature, but the mechanism of action is still controversial. Besides, limited information was presented on the antibacterial mechanism of MgO and CaO in the literature. In this study, DMPO spin trapping characteristics of MgO and CaO in ESR technique was investigated for a deeper understanding. Oxygen radical amount, which was generated from the ZnO powders and the ZnO containing textile surface, was determined. It was thought that clarifying of the antibacterial mechanism of metal oxides would lead to develop faster and cheaper antibacterial test methods instead of conventional methods.

Experimental

Base Fabric

100 % polyester, 295 g/m^2 plain weaved (12.5 yarn/cm warp, 9.5 yarn/cm weft) fabric was used for coating applications. Warp yarns were 1670 dtex multiflament yarns and weft yarns were monofilament yarns with 0.25 mm diameter.

Coating Applications

Coating applications were performed with ATAC (Istanbul, Turkey) laboratory type coating machine and curing processes were carried out at 180 ^oC for 2 minutes with ATAC GK40 (Istanbul, Turkey) laboratory type textile dryer. Direct coating method was applied. The chemicals used in

Table 1. The chemicals used in coating applications

Chemical type	Usage amount (%)
PVC	54.17
Plasticizer 1	33.17
Plasticizer 2	6.77
Epoxidized soybean oil	1.03
Antifoam agent	0.54
Viscosity adjuster	2.71
Thermal stabilizer	1.60
Metal oxide	X %

coating applications were given on Table 1.

Plasticizers are suitable to food contact, Plasticizer 1 is adipic acid and polyhydric alcohol mixture and Plasticizer 2 is acetyltributylcitrate derivative. Viscosity of the polymer paste without metal oxide addition was 26000±3000 cP which is determined by Brookfield viscometer (Massachusetts, USA).

Metal oxides at proper concentration were added during polymer paste preparation. Polymer paste was prepared with IKA (Staufen, Germany) mixer at 1500 rpm for 15 minutes. Mixed polymer pastes were then left in 0.2 bar vacuum for 30 minutes for bubble removal. One and double layered coating construction was carried out. At higher metal oxide concentrations (higher than about 3 %) the structure of the coating became brittle and risk of deterioration on mechanic properties was emerged for practical use. Therefore, metal oxides were added to thin second layer which is planned to be antibacterial layer. By this way, high metal oxide loading (up to 35 %) to polymer paste was possible without damaging mechanical properties for practical use. The thickness of base coating was 0.8 mm where the second metal oxide containing layer was 0.25 mm.

Zinc oxide concentrations were 10-35 %, calcium oxide concentrations were 5-35 % and magnesium oxide concentrations were 5-25 %.

Metal Oxide Powders

Zinc oxide (ZnO-Sigma Aldrich), calcium oxide (CaO – Sigma Aldrich) and magnesium oxide (MgO (heavy) – Merck) were used as antibacterial agents. All metal oxide powders used in the experiments were in analytical grade.

Antibacterial Tests Applied to Coated Samples

Antibacterial tests were performed according to ISO 22196-2011 standard. *Listeria innocua* NRLL-B 33314 species were used as test bacteria. Though *L. innocua* is not a human pathogen, detection of *L. innocua* on an environment is an important indicator for presence of pathogen *Listeria* species such as *L. monocytogenes.* Also, *L. innocua* can be used for model bacteria instead of *L. monocytogenes* for antibacterials tests [42]. The mean values of three antibacterial tests for each specimen were given as the antibacterial activity results.

Antibacterial efficiencies of 5, 10 and 20 times washed samples were also tested. Washing procedure was developed regarding industrial applications [43]. Each washing cycle consisted of one-minute aggressive washing with sponge and 20 seconds of cold rinsing. 4 g/*l* ECE A standard reference detergent was applied at washing step.

ESR Measurements

ESR measurements were performed with Bruker e-scan model X-band spectrometer (Ettlingen, Germany) with following conditions: Microwave frequency, 9.80 GHz; scan width 65G; receiver gain 1.26×102; resolution 512; conversion time, 81.92 msec; time constant 655 msec; scans, 2; modulation frequency, 86 kHz.

0.02 M DMPO (dimethylpyrroline-N-oxide) spin trap (Sigma-Aldrich) was used to detect ROS in ESR. DMPO can be utilized to trap both hydroxyl and superoxide radicals giving DMPO-OH and DMPO-OOH spin adducts, respectively, however, DMPO-OOH is unstable and converted to DMPO-OH in time [34,44]. A calibration curve was generated with the signal areas of known concentrations (0.1, 1, 2, 5, 10, 20, 30 μM) of TEMPO (2,2,6,6-tetramethylpiperidine 1-oxyl) (Sigma-Aldrich) stable radical. Signal areas were calculated by double integration of the first derivative of ESR signals. The oxygen radical concentrations were calculated by means of this calibration curve, using the signal areas of DMPO-OH spin adduct signal [35,36,45,46].

Liquids were sampled t in capillary glass tubes, then placed into ESR tubes for measurement. All chemicals used as supplied, no further purification was carried out. Ultrapure water (18.3 MΩ) was used for the experiments.

360 nm UV light was applied to samples for 30 minutes in the experiments that the influence of UV light was investigated.

Y axis represents signal intensity (a.u.) and X axis represents magnetic field (mT) in the figures which exhibit ESR signals

DCFH-DA Experiments

Thermo Fisher Scientific Varioskan Flash microplate reader (Massachusetts, USA) and Zeiss Axio Observer Z1 fluorescent microscope (Oberkochen, Germany) were used to observe intercellular oxidative stress caused by metal oxides using DCFH-DA. The increase of the fluorescence would be an indicator of increased oxygen radical amount.

96-well black microplate (Thermo Fisher) was used for microplate reader measurements. 300 μ*l* growth medium which contained 2.5×10^7 CFU/m*l* bacteria, 30 g/*l* soy broth (Merck) and 100 g/*l* metal oxide was prepared inside wells. After incubation of 3 hours at 37 °C, 100 μ*l* DCFH-DA (Fluka) in DMSO (dimethyl sulfoxide, Sigma) solution was added to culture medium and the total concentration of DCFH-DA in the well was adjusted 100 μM. The incubation was carried out for another 1 hour at the same conditions. After incubation, microplate was fluorimetricly scanned in microplate reader. Excitation and emission wavelengths were λ_{ex}=498 nm, λ_{em}=522 nm, respectively. The mean values of three measurements were calculated.

The samples then transferred to UV-transparent 96-well microplate (Thermo Fisher) in a sterile environment for fluorescent microscope measurements. Microscope images were taken with 40x lens. Excitation and emission wavelengths were λ_{ex}=504 nm and λ_{em}=525 nm, respectively. Exposure time was 8.4 ms.

Fluorescein Experiments

Sodium salt of fluorescein (Fluka) was used. 10^{-5} M fluorescein solution in ultrapure water was interacted with metal oxide powders for 1 or 24 hours. Metal oxide-fluorescein suspensions were centrifuged for 20 minutes at 2000 rpm after interaction. Supernatants were collected and the change on the absorbance of fluorescein solutions were monitored in quartz cells between 300-700 nm by Perkin-Elmer Lambda 35 UV-vis spectrometer (Massachusetts, USA).

The metal oxide concentrations were varied between 1-100 g/*l*. 360 nm UV light was applied to samples in the experiments that the influence of UV light was investigated.

Particle Size Analyses

Particle size of metal oxide powders were determined with dynamic light scattering method using Malvern Zetasizer (Malvern, UK). Propane-2-ol (Sigma), ethylene glycol (Sigma) and pure water were dispersant mediums for calcium oxide, zinc oxide and magnesium oxide, respectively.

SEM Images and EDX Analyses

The surface morphology of coated samples and distribution of metal oxide particles on the surface were investigated with SEM images and EDX analyses which were carried out by FEI QUANTA 250 FEG electron microscope (Oregon, USA).

FT-IR Analyses

FT-IR studies were carried out by Perkin-Elmer Spectrum Two FT-IR spectrometer (Massachusetts, USA). The spectra were acquired 450-4000 cm^{-1} range with 4 cm^{-1} resolution.

Determination of Coating Thickness and Add-on

Mitutoyo (Illinois, USA) thickness gauge was used to measure coating thickness. Add-on was calculated according to following formula:

$$\%W_{\text{add-on}} = \frac{W_1 - W_2}{W_1} \times 100 \quad (1)$$

where, $W_{\text{add-on}}$: total add-on, W_1: mass before coating, W_2: mass after coating.

Results and Discussion

Particle Size Distribution of Metal Oxide Powders

As mentioned earlier, direct contact of the bacteria and the metal oxide is a very important parameter for the antibacterial effect. Considering the size of bacteria (0.4-0.5 μm×0.5-2 μm for *Listeria* species) [47], the applied metal oxide powder should be dispersed on the coating surface properly leaving no space for bacterial reproduction. At this point, particle size of metal oxide is an important parameter. The particle size distributions of calcium oxide magnesium oxide and zinc oxide were shown on Figure 1.

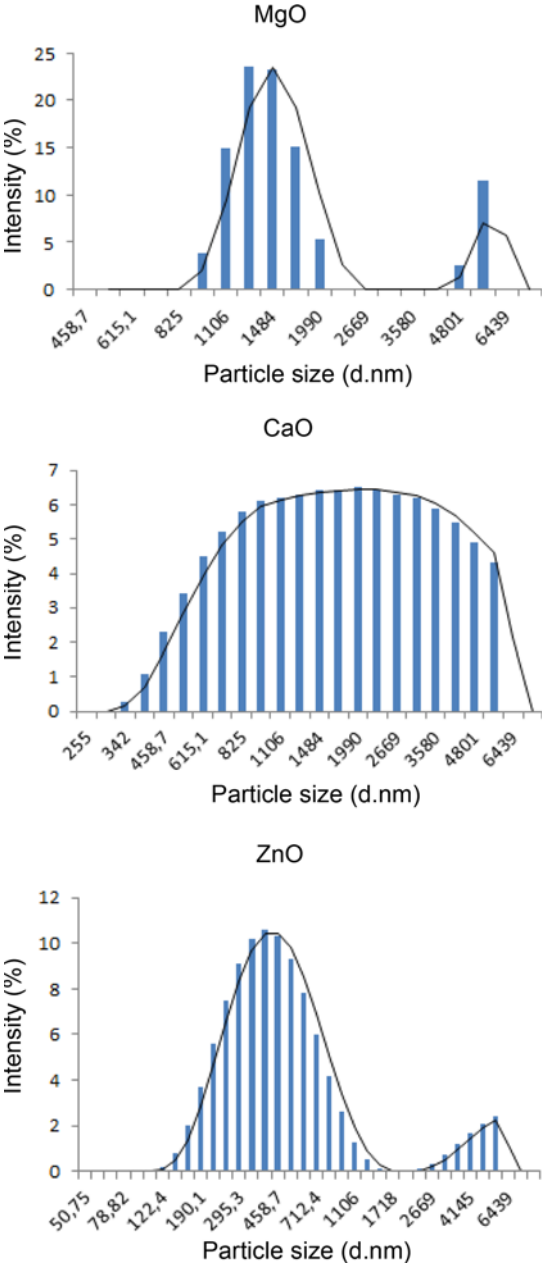

Figure 1. Particle size distribution of used metal oxides.

The particle sizes of magnesium oxide particles did not vary in a wide range, the particle diameters were generally between 955-1990 nm. It is thought that particle diameters detected between 4800-5560 nm was a result of agglomeration. Likewise, agglomeration originated particles detected for zinc oxide powders around 3500-5500 nm particle size. The mean zinc oxide particle size was 378 nm. particle size distribution of calcium oxide was varied between 400-5600 nm. The mean particle size of calcium oxide was about 1400 nm.

SEM Images and EDX Analysis

SEM images and EDX analyses are important tools to determine metal oxide distribution on the surface which is a crucial parameter for strong antibacterial effect and repeatability. Homogenous and dense distribution of metal oxide particles on the coating surface is the aimed ideal situation. SEM image and EDX mapping of control sample were shown on Figure 2. The EDX analysis results were presented on Table 2.

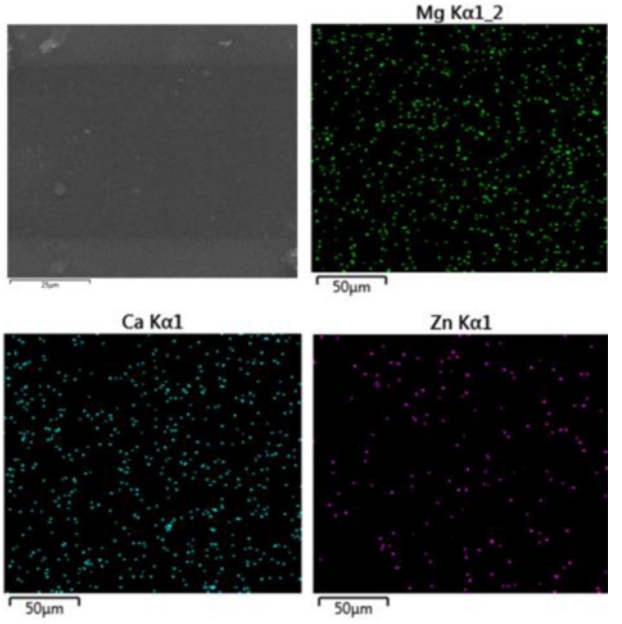

Figure 2. SEM image and EDX mapping of Mg, Ca and Zn atoms of control sample.

Table 2. EDX analysis of control sample

Element	Mass ratio (%)	Atomic ratio (%)
C	69.55	81.76
O	12.62	11.14
Cl	17.75	7.07
Mg	0.02	0.01
Ca	0.06	0.02
Zn	0.00	0.00

Negligible amount of Mg, Ca and Zn atoms were detected on the control sample. EDX data was corrected with the EDX maps that exhibited no significant Mg, Ca or Zn atom existence on the control sample surface. The distribution of metal oxides is clearly seen on Figure 3.

The first thing drew the attention on the SEM images was the homogeneous distribution of metal oxides on the coating surface. As things stand, metal oxides did not bury into the

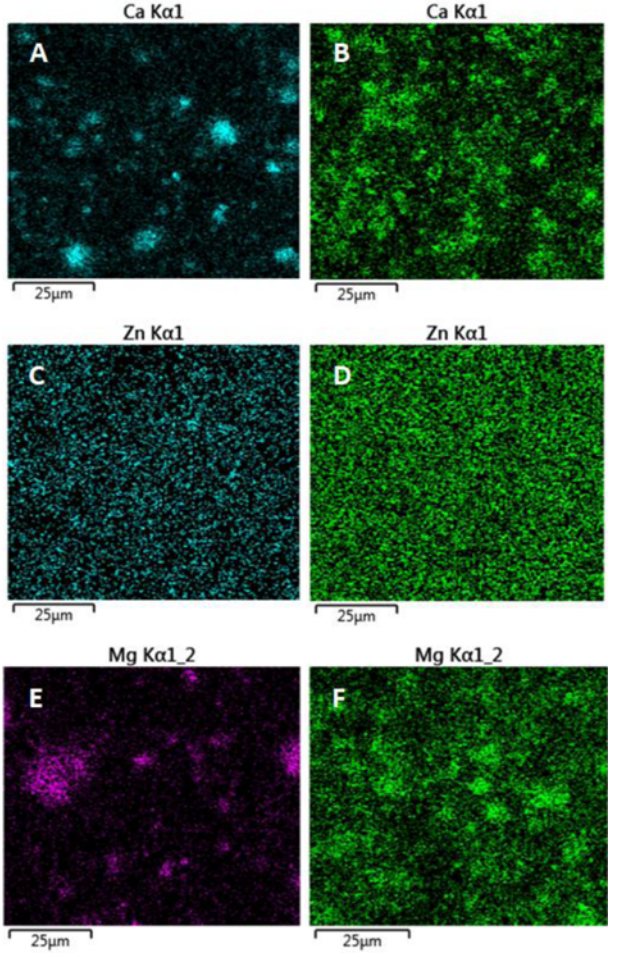

Figure 4. EDX maps of metal oxide containing samples; (A) 5 % CaO, (B) 20 % CaO, (C) 10 % ZnO, (D) 35 % ZnO, (E) 5 % MgO, and (F) 20 % MgO.

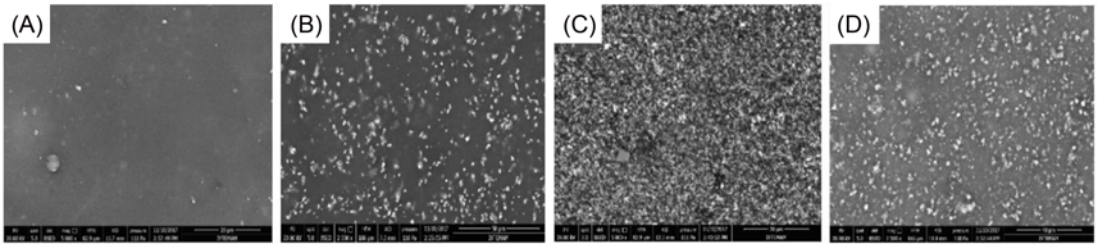

Figure 3. SEM images of control sample and metal oxide containing samples; (A) control, (B) 20 % CaO, (C) 35 % ZnO, and (D) 20 % MgO.

polymer which would lead them remaining idle, nothing but a filler material. It was thought that, dense and quite proper location of antibacterial agents would provide a repeatable and strong antibacterial activity. EDX maps were proved this homogeneity in atomic manner with zinc, calcium and magnesium atom scans. Also, owing to EDX mappings, the effect of concentration to the metal oxide distribution on the coating surface was observed. EDX mappings belonged to metal oxide containing samples were shown on Figure 4.

The agglomeration tendency is observed for magnesium oxide and calcium oxide especially at 5 % concentration. This situation was also monitored with particle size analysis. As expected, higher concentrations avoid sparse location of metal oxides on the surface and brought in more homogenous distribution. The metal oxide amount and distribution on the surface varied depending on concentration would affect antibacterial behavior of the coated sample.

Antibacterial Efficiency of Coated Samples

Thus, first studies were focused on one-layered metal oxide containing coating. Magnesium oxide, zinc oxide and calcium oxide concentrations were varied between 0.3-1.5 % at one-layered coating studies. Even though antibacterial activity was observed at these concentrations (up to 84 % for 0.7 % MgO concentration), some repeatability problems were observed (data not shown). Close contact between metal oxide and bacteria is a vital parameter for antibacterial activity [11]. In case of our experiments, sparse metal oxide particle presence on the surface might be the reason of the problem, since, encounter probability between metal oxide and bacteria was decreased.

It is thought that, direct addition of the active material to the polymer paste and coating textile material with this recipe forming one polymer layer is the easiest and the most economical way to add function to a coated textile material.

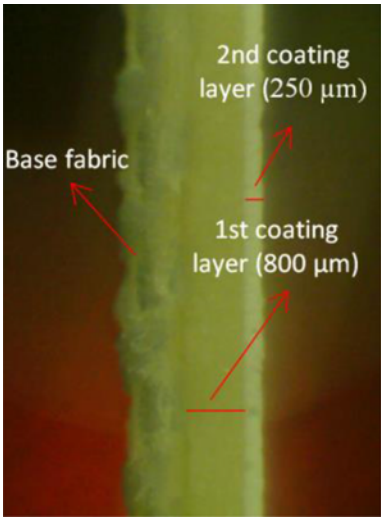

Figure 5. Two-layered coating structure.

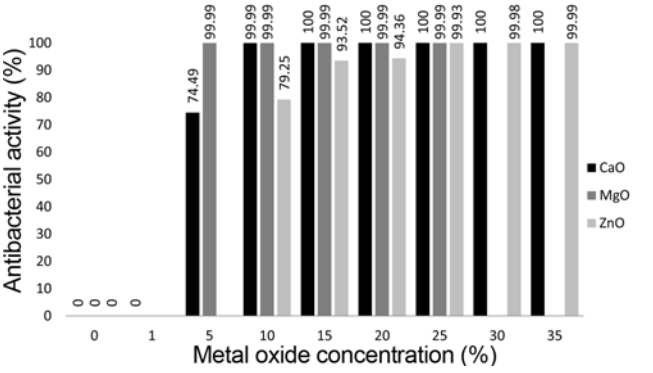

Figure 6. Antibacterial activity of metal oxide containing coated samples.

However, in one-layered coating, high concentration (above 3 %) of metal oxide loading to the polymer paste resulted in brittle coating structure. Therefore, metal oxide containing functional thin second layer coating was applied to coated material which was formerly coated with the standard recipe without metal oxide addition. Two-layered coating structure is seen on Figure 5. By this method, both the mechanical deterioration was avoided and high concentration of metal oxide addition was possible. The antibacterial activities of two layered coated samples depending on metal oxide type and concentration are seen on Figure 6.

The thickness of first layer and second layer were 800 µm and 250 µm, respectively. The add-on values were 15.6 % for CaO, 18.0 % for ZnO and 16.7 % for MgO containing second layer coatings.

Applied standard obligates to perform the test on at least 3 samples; therefore, these results are the mean values of three measurements. Bacterial growth on the cultures of the control samples that did not contain metal oxide were healthy and no contamination trace was detected, indicating that the antibacterial effect would be originated from metal oxide existence.

10 % zinc oxide containing samples exhibited around 80 % antibacterial activity. It is seen on Figure 2 that the antibacterial efficiency of zinc oxide containing coated samples is concentration dependent, the higher the concentration, the higher antibacterial activity was observed. A dramatic rise on the antibacterial activity (around 93 %) was determined for 15 % zinc oxide containing sample, comparing with 10 % zinc oxide containing sample. The highest antibacterial activity (99.9 %) among zinc oxide containing samples was achieved with 35 % concentration.

99.9 % antibacterial activity against *L. innocua* species was detected for magnesium oxide containing samples for all concentrations (5-25 %) investigated in this study. It is thought that maximum antibacterial yield is achieved with 5 % magnesium oxide concentration against *L. innocua* and further development (100 % antibacterial activity) could not

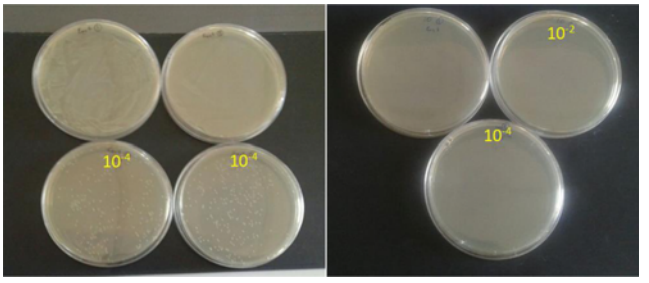

Figure 7. Petri dishes belonged to the antibacterial test of 10 % calcium oxide containing sample (control sample on the left, 10 % CaO sample on the right) (dillution amounts are noted on the petri dishes).

be possible. Higher concentrations might be effective against other pathogen species.

No antibacterial activity was detected against *L. innocua* with 1 % calcium oxide concentration. On the other hand, 5 % calcium oxide provided quite high efficiency with 74.5 %. For a satisfactory protection, an antibacterial product, especially a conveyor belt should eliminate almost all, if it is possible entire pathogens in the environment, since, surviving bacteria always will be a source of risk for cross contamination. 99.99 % antibacterial efficiency was provided by 10 % calcium oxide concentration. Concentration dependent results were perceptible when metal oxide distribution on the surface was monitored (Figure 3). Petri dishes belonged to the antibacterial test of 10 % calcium oxide containing sample are presented on Figure 7.

15 % and above concentrations exhibited 100 % antibacterial activity, which means no CFU was detected after 24 hours of incubation. Even though 15 % concentration provide 100 % antibacterial activity against *L. innocua*, higher concentrations might answer to the protection needs against other pathogen species.

At this point, a problem about mechanical properties of calcium oxide containing coated samples should be underlined. Higher calcium oxide concentration than 20 % (25, 30 and 35 %) caused brittle structure resulted in inflection of the material. Thus, calcium oxide usage above 20 % is not recommended under the conditions of this study. The reasons of this phenomenon will be investigated in depth later on.

Effect of Contact Time

Standard antibacterial tests generally require 24 hours of contact between bacteria and test specimen under certain incubation conditions. However, in a dynamic environment such as an industry facility, the elapsed time for antibacterial influence of the antibacterial industrial textile material is important. For this reason, the required time for maximum efficiency was investigated. Test were applied with the standard test conditions, however, contact times were varied. The changes on the antibacterial properties depending on contact time were presented on Figure 8.

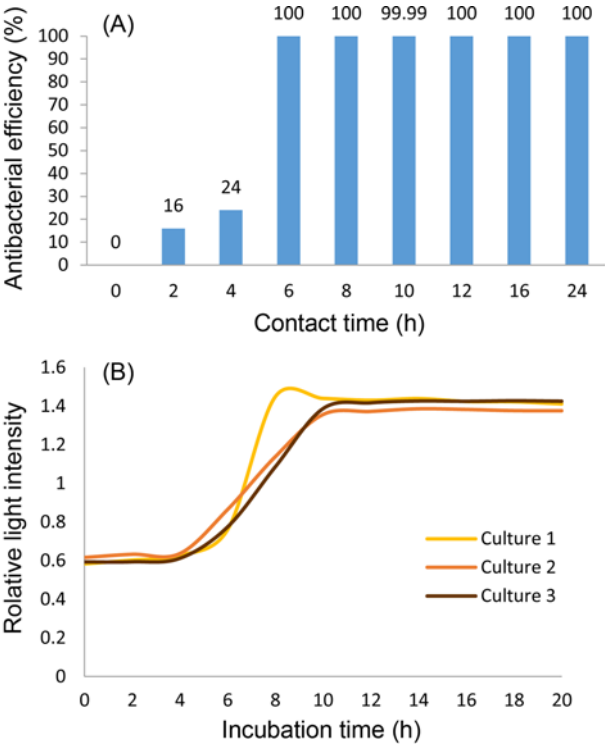

Figure 8. Effect of contact time on the antibacterial efficiency; (A) time dependent antibacterial activity of 20 % calcium oxide containing sample and (B) growth curves of *Listeria innocua* acquired in 20 hours.

Growth stages of bacteria are generally divided as adaptation phase (lag phase), logarithmic reproduction phase (log phase) and stationary phase. These three phases are able to seen on *L. innocua* growth curves. The effect of contact time between 20 % calcium oxide containing sample and bacteria growth curve could be matched. No antibacterial effect was determined for zero contact (bacterial culture was spread on the sample and collected from the sample instantly). At 2 and 4 hours of contact, antibacterial activity started to be observed, however, remained limited. It seemed that the effect of the antibacterial material remained limited during lag phase of the growth circle. A sharp increase was observed on the antibacterial efficiency at 6 hours contact time which corresponded to the beginning of the log phase. After 6 hours, antibacterial activity was determined 100 % for investigated contact times, except 10 hours (99.9 % antibacterial activity). If the growth curve is checked, log phase ends at tenth hour and subsequently, stationary phase is started. Produced antibacterial coated textile material possibly most interrupted the reproduction mechanism of the bacteria.

Effect of Washing on Antibacterial Efficiency

Similar procedures with industrial washing applications were carried out to metal oxide containing (35 % ZnO,

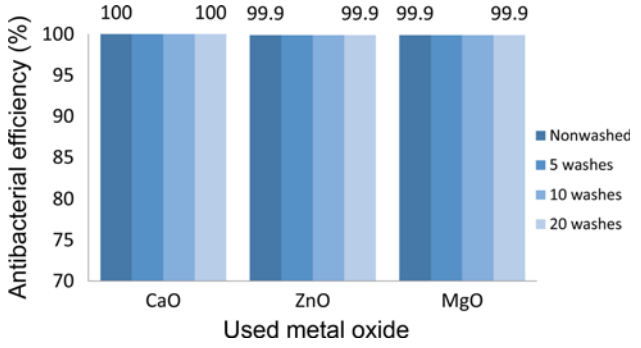

Figure 9. Change on antibacterial activity depending on washing.

20 %CaO, 20 % MgO) coated samples. Antibacterial properties need to be kept after serial washings for long term service in the practical use. The changes on antibacterial efficiency with washing procedures were shown on Figure 9.

No decrease was recorded on the antibacterial properties of metal oxide containing coated samples after 5, 10 or 20 times washing. This results indicated sufficient adherence of metal oxides on the PVC polymer surface that they could not be removed with 20 times washing.

Investigation of Antibacterial Mechanism with DCFH-DA Assay

As explained earlier, DCFH-DA assay is a useful tool for determination of intercellular oxidative stress. Using this technique facilitated us to evaluate relative oxygen radical amount released due to metal oxide catalytic reactions. The experiments were carried out under dark conditions. Fluorimetric microplate reader measurements of bacteria interacted with metal oxides under DCFH-DA existence were presented on Figure 10.

The fluorescence intensities of DCFH-DA free samples were close to each other and very low. The fluorescence intensities of the metal oxide containing samples were slightly higher than control sample. The metal oxide

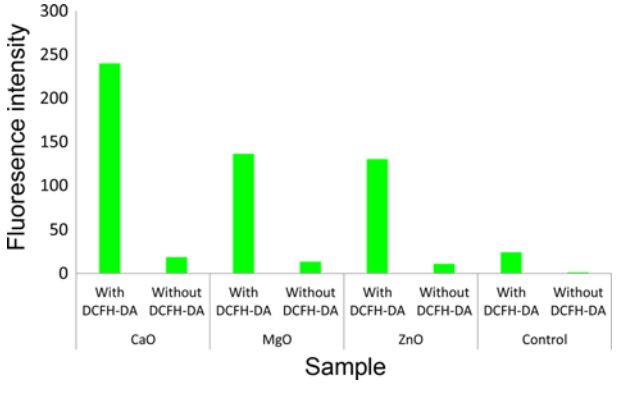

Figure 10. Microplate reader fluorometric measurements with DCFH-DA.

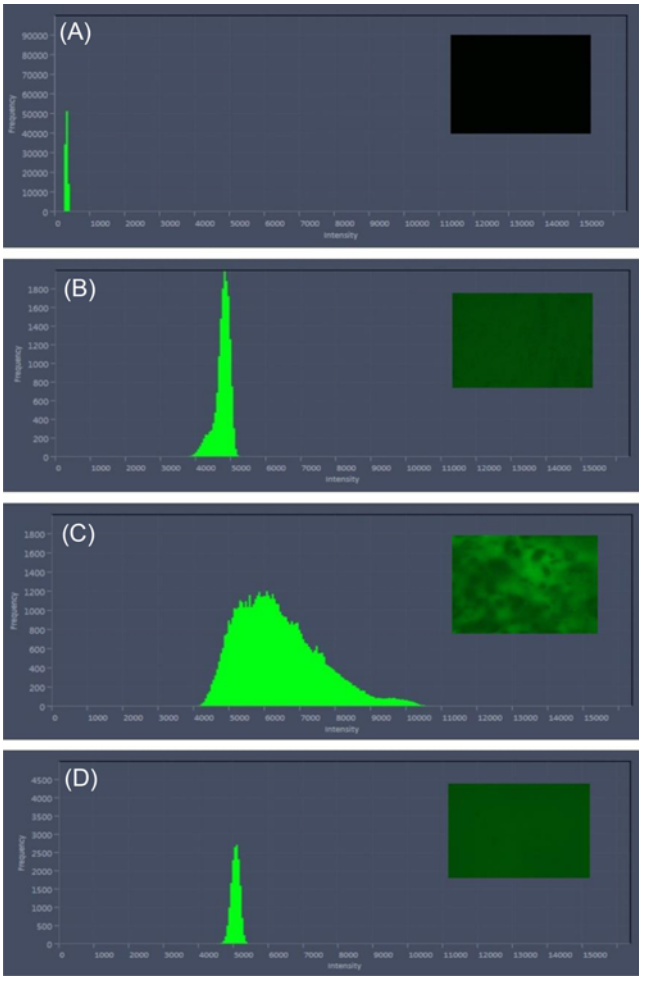

Figure 11. Fluorescent microscope images and fluorescent intensities of metal oxide, bacteria and DCFH-DA containing samples obtained by fluorescent microscope; (A) control, (B) CaO, (C) ZnO, and (D) MgO.

existence might be the reason of this faint increase on the fluorescence, in the absence of DCFH-DA. An increase on the fluorescence of DCFH-DA containing control sample was detected, which is thought to be the result of the oxygen radicals released during bacterial metabolism activities. On the other hand, fluorescence intensities of metal oxide and DCFH-DA containing samples were remarkably increased. The fluorescence intensity of calcium oxide containing sample increased by 10 times compared to the control. The increase was 460 % for magnesium oxide and 440 % for zinc oxide containing samples. These results confirmed ROS formation in the presence of calcium oxide, zinc oxide and magnesium oxide. While, 100 % antibacterial efficiency was attained by calcium oxide containing samples, the maximum antibacterial efficiency was 99.9 % with zinc oxide and magnesium oxide. It is thought that the higher oxygen radical releasing might be the reason of the higher

antibacterial activity of calcium oxide among others.

The results obtained by fluorescent microscope were in parallel line with the microplate reader results. The fluorescent microscope images and fluorescence intensities were shown on Figure 11.

Small amount of ROS due to the metabolic activities of cells were detected by the slight fluorescent intensity of the control sample, compatible with the microplate reader measurements. Though the bacteria were unable to seen on the fluorescent microscope images, background fluorescence was clearly visible for metal oxide containing samples. Also, fluorescence intensities were dramatically increased for both calcium oxide, zinc oxide and magnesium oxide containing samples. Since DCF is a nonselective probe, discrimination of the kind of oxygen radicals came to exist is very hard, however, fluorescent microscope images and fluorescent intensity data obtained from fluorescent microscope measurements indicated oxygen radical presence. The data collected from DCFH-DA experiments, either microplate reader or fluorescent microscope are interpreted as calcium oxide, zinc oxide and magnesium oxide caused oxidative stress in *Listeria innocua* species.

Investigation of Antibacterial Mechanism with Fluorescein Assay

A strong absorbance peak was observed on UV-vis spectrometer measurements of fluorescein around 490 nm wavelength. The changes on the absorbance of fluorescein interacted with 10-100 g/*l* CaO for 24 hours are seen on Figure 12.

Interaction of fluorescein with CaO resulted in decrease on the absorbance of fluorescein. It was observed that the decrease amount was concentration dependent for CaO interaction, the higher the concentration, the higher the fall was detected. A slight fading was determined for 10 g/*l* CaO concentration on the absorbance at 491 nm. On the other hand, 100 g/*l* CaO resulted in 28 % decrease on the absorbance of fluorescein at 491 nm. From these results, it is obvious that CaO caused notable degradation of fluorescein. Considering the data obtained from DCFH-DA assay which oxygen radical formation was detected due to CaO existence, it is thought that CaO caused the degradation of fluorescein by direct catalytic reactions or oxygen radical formation. UV light exposure did not have any influence on fluorescein and 10 % CaO interaction (data not shown). It was thought that, due to the high band gap energy of CaO, photo excitation with the UV light source used in this study could not be possible.

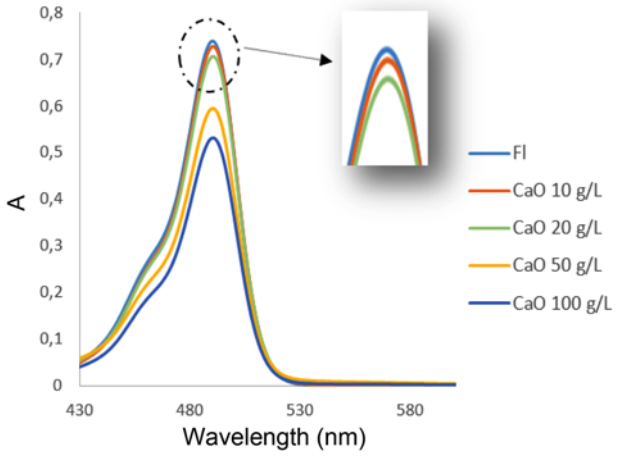

Figure 12. The changes on the absorbance of fluorescein interacted with CaO powder.

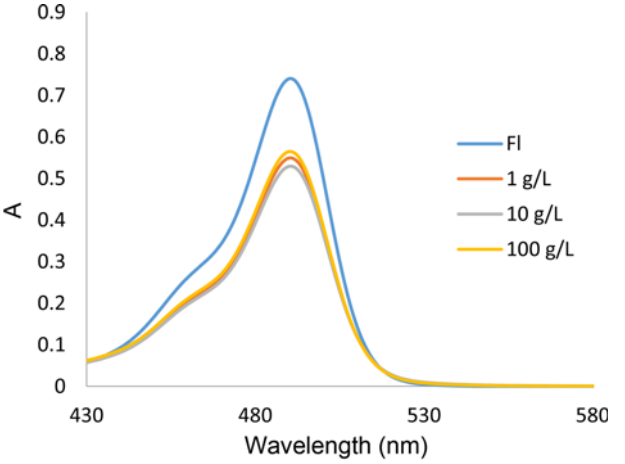

Figure 13. The change of absorbance of fluorescein in the presence of zinc oxide under UV light.

Apart from magnesium oxide and calcium oxide, zinc oxide is a semiconductor material with relatively low bandgap (3.2 eV) and can be activated with UV or visible light photon energy owing to its electronic structure. This feature brings in photocatalytic reaction abilities to zinc oxide. Zinc oxide is not only active with light excitation, but also active under dark conditions. In this study ZnO was interacted with fluorescein under UV light and dark. The catalytic activity of ZnO was monitored with the fading of the absorbance of the fluorescein. No significant change was detected on the absorbance of fluorescein interacted with 100 g/*l* ZnO for 24 hours under dark conditions (data not shown). The effect of different concentrations of ZnO on the absorbance properties of fluorescein was shown on Figure 13.

The peak at 491 nm on the absorbance spectrum of fluorescein notably decreased after ZnO treatment under 1 hour of UV light exposure. The quenching of fluorescein in the presence of ZnO under 360 nm UV light seemed to be independent from ZnO concentration. There was a negligible difference between the decrease of the absorbance of 10^{-5} M fluorescein solutions that interacted with 1, 10 and 100 g/*l* ZnO. Our findings were in parallel line with Bardhan *et al.* [40], who determined the degradation of fluorescein in the

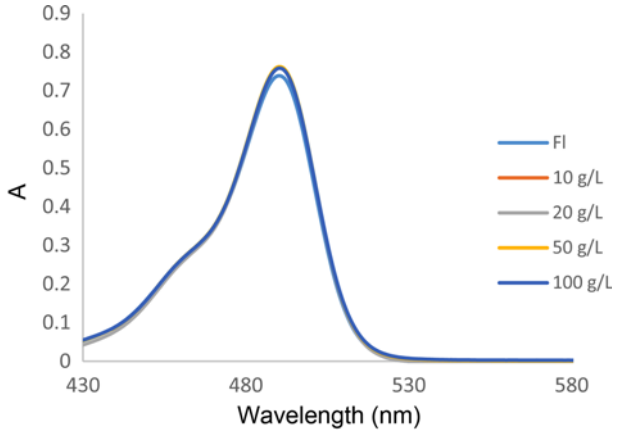

Figure 14. The change of absorbance of fluorescein interacted with magnesium oxide powder for 24 hours.

presence of ZnO nanoparticles and stated that the quenching of fluorescein might be attributed to energy electron transfer process between ZnO and fluorescein or oxygen radical formation due to the photocatalytic process. Considering the DCFH-DA assay results, it is thought that oxygen radical formation has an important role on the quenching of fluorescein, however direct catalytic reactions might also be involved to the process.

10 g/*l* magnesium oxide did not affect the absorbance of fluorescein under 1 hour of UV light exposure. Also, 24 hours of interaction between magnesium oxide in varied concentrations (1-100 g/*l*) and fluorescein did not cause any quenching. Absorbance spectra of fluorescein solutions interacted 24 hours with varied concentrations of MgO was shown on Figure 14.

Though, ROS formation detected in the presence of MgO with DCFH-DA assay, MgO did not cause to quenching of the fluorescein dye. Likewise, ZnO could not degrade fluorescein molecule under dark conditions, regarding the UV-vis absorbance spectrum. At this point, DCFH-DA microplate reader experiments should be recalled. If Figure 10 is checked, the relative fluorescence intensities of MgO and ZnO were very close to each other and one should keep in mind that DCFH-DA assay performed under dark conditions. From these results, it was thought that the amount of oxygen radical formed in the presence of MgO and ZnO under dark conditions was insufficient for the degradation of fluorescein molecule at detectable range of UV-vis spectrometer at investigated conditions.

ESR Analyses with Zinc Oxide

As explained earlier, ESR technique is a useful tool to study radical species such as oxygen radicals. In this study, ESR spin trapping technique was carried out to observe

Figure 16. ESR spectrums of DMPO spin trap and different concentration of ZnO suspensions interacted under dark conditions (A) or UV light exposure (B).

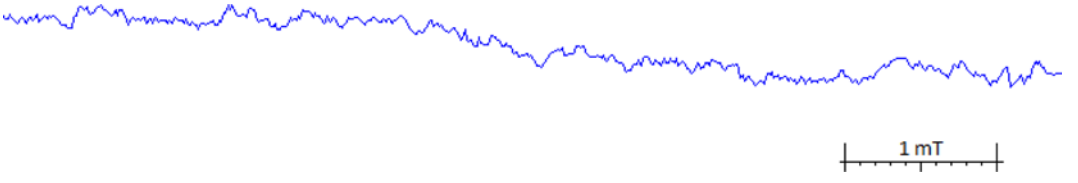

Figure 15. ESR spectrum of blank DMPO solution.

oxygen radical formation and quantification of oxygen radical amount released due to the metal oxide existence. Primarily, oxygen radical formation behavior of calcium oxide, zinc oxide and magnesium oxide powders was analyzed. Subsequently, oxygen radical releasing of coated fabrics was investigated. A calibration curve was created by the virtue of ESR signal areas of known concentrations of TEMPO spin label. Oxygen radical amounts were determined by using this calibration curve and comparing signal areas of DMPO-OH spin adduct ESR spectrum.

ESR technique is used in many scientific fields such as physics, chemistry, medicine, nuclear researches, polymer science and so on. It is thought that, apart from this study, ESR technique would provide solutions with many applications on textile researches.

ESR spectrum of blank DMPO solution was shown on Figure 15.

As expected, no signal trace related to DMPO-OH spin adduct was determined on the ESR spectrum of blank 0.02 M DMPO solution. Therefore, further detected signals would be induced by the metal oxide existence. The ESR spectrums recorded after DMPO and different concentrations of ZnO interaction under dark conditions or UV light exposure was shown on Figure 16.

ZnO induced ROS formation was successfully detected using DMPO spin trap. Characteristic quartet signals of DMPO-OH spin adduct were identified for ZnO suspension of various concentrations. DMPO is able to trap both $^{\bullet}OH$ and O_2^- radicals producing DMPO-OH and DMPO-OOH spin adducts, respectively. However, DMPO-OOH is unstable and decomposes to DMPO-OH [44,45]. Therefore, obtained signals were originated from hydroxyl and superoxide radicals released by ZnO particles.

Oxygen radical presence was detected for 1, 10 and 100 g/*l* concentrations of suspended ZnO, without light excitation. Though, ROS generation of metal oxides without light exposure is still a controversial issue, owing to its electronic structure, zinc oxide gets involved to catalytic reactions without needing light [31]. Another possible factor that enables metal oxide to generate ROS is surface defects such as oxygen vacancies [19,20,45]. Oxygen radical generation under dark conditions was also stated by Prasanna and Vijayaraghavan [20], Hirota *et al.* [16], Applerot *et al.* [45] which is consistent with our findings. The significant increase on the signal intensities with UV light is apparent on Figure 16. The photocatalytic reactions of zinc oxide resulted in higher amount of oxygen radical generation due to the electron-hole couple formation ruled by photon energy.

Oxygen radical generation from different zinc oxide concentrations under dark or UV light conditions can be more accurately compared with the calculation of released oxygen radical amount. To calculate oxygen radical amount, a calibration curve created by the signal areas of known concentrations of TEMPO stable radical was utilized. The calibration curve used for oxygen radical amount calculations was shown on Figure 17.

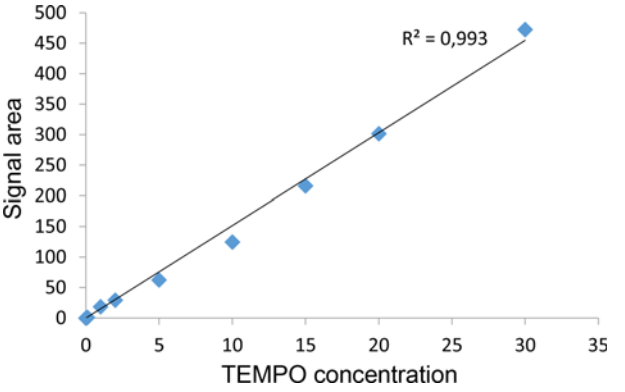

Figure 17. Calibration curve created with the signal areas of known concentrations of TEMPO.

0.3 μM oxygen radical amount was calculated for 1 g/*l* ZnO without light excitation. This was the lowest value among investigated zinc oxide samples. 1.15 and 0.82 μM oxygen radical generation detected for 10 and 100 g/*l* zinc oxide suspensions in the dark, respectively. The effect of UV light on the released oxygen radical concentration was remarkable; calculated oxygen radical amounts were 7.78 μM, 7.67 μM, 7.82 for 1, 10 and 100 g/*l*, respectively. The important point here was that oxygen radical amounts remained almost same as the zinc oxide concentrations raised. Consistent results were observed in the fluorescein experiments performed under UV light with ZnO (Figure 13). Zinc oxide is not soluble in water. So, the area of suspended zinc oxide activated by UV light might have been limited. Another reason for this phenomenon could be the limited attraction between water and zinc oxide powder due to the same solubility problem.

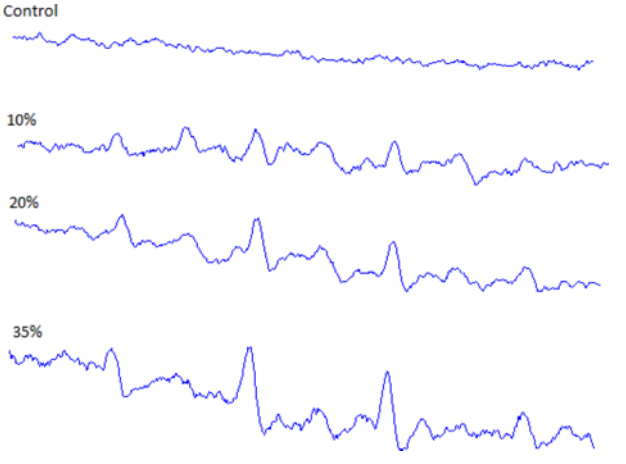

Figure 18. ESR spectrums of 0.02 M DMPO solutions interacted with zinc oxide containing PVC coated samples.

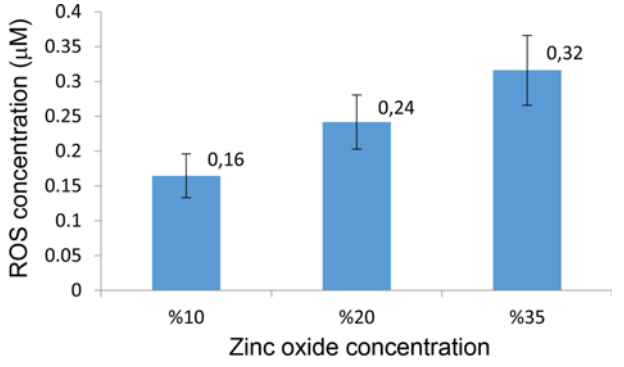

Figure 19. Oxygen radical concentrations determined on zinc oxide containing samples.

Due to the small amount of ZnO on the coated textile surface, ESR spectrum of DMPO-OH was unable to detect after 30 minutes of DMPO-ZnO interaction in the dark. ESR spectrums obtained after 30 minutes of UV illumination from 10, 20 and 35 % zinc oxide containing coated surfaces were presented on Figure 18. Since the signal intensities raised with light energy, UV light was used as an accelerator for the process.

Signal intensities of DMPO-OH samples collected from zinc oxide containing samples increased. To establish a more accurate relationship between oxygen radical generation and antibacterial activity, oxygen radical amounts released from coated sample surfaces were determined. Calculated released oxygen radical amounts were shown on Figure 19.

The rise of antibacterial efficiency depending on the zinc oxide concentration and the increase of oxygen radical amounts generated on coated samples' surfaces exhibited parallel behavior. The antibacterial activities of 10, 20 and 35 % zinc oxide containing samples were 79.25 %, 94.36 % and 99.99 % (Figure 6), respectively. The determined ROS concentrations were 0.16 (10 % ZnO), 0.24 (20 % ZnO) and 0.32 (35 % ZnO) µM for the same samples. The signal areas are the main values of ten measurements and standard deviations of signal areas were 0.03, 0.04 and 0.05 for 10 %, 20 % and 35 % zinc oxide containing samples, respectively. It was thought that obtained results were important sign for the correlation between antibacterial activity and ROS generation. Acquired data from present study might lead future studies focused on developing new antibacterial test methods depending on the antibacterial mechanism.

ESR Analyses with Magnesium Oxide and Calcium Oxide

ESR spectrums of DMPO solutions interacted with MgO in the dark or under UV light were presented on Figure 20.

Characteristic quartet signal of DMPO-OH spin adduct could not be observed with MgO interaction of DMPO, however, triple signals, analogue of TEMPO were obtained. Fiedot *et al.* [17] stated that high amount of peroxide

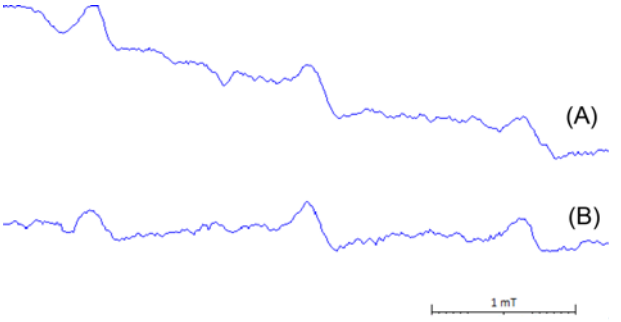

Figure 20. ESR spectrums of DMPO solutions interacted with MgO in the dark (A) and under UV light (B).

presence leads to oxidation of DMPO giving nitroxyl radical which has triple ESR signals. This statement explains the similarity with the TEMPO signal, since TEMPO is a nitroxyl radical. Based upon these results, it was thought that due to the oxygen radical generation or via direct catalytic reactions, MgO resulted in the oxidation of DMPO spin trap. Thus, oxygen radical concentration determination could not be possible. There is no significant effect of UV light on the reaction of MgO with DMPO. Possibly, applied UV light had no influence on the reactivity due to the relatively high

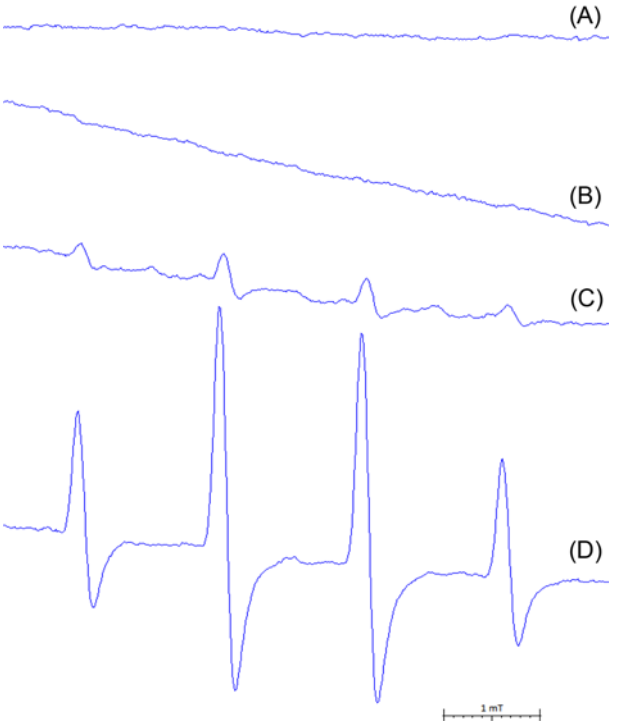

Figure 21. The effect of CaO on the DMPO spin trap; (A) ESR spectrum of CaO-DMPO interaction, (B) ESR spectrum of under UV light interaction between ZnO-DMPO that was pretreated with CaO, (C) ESR spectrum of interaction between ZnO-DMPO under UV light at pH 12.6, and (D) ESR spectrum of ZnO-DMPO interaction under UV light.

band gap (around 7.8 eV [48]) of MgO.

No oxygen radical generation was detected with ESR method using DMPO spin trap in the presence of CaO. This result was incompatible with former findings obtained with DCFH-DA and fluorescein assays. The marks of the oxygen radical generation and catalytic activity of CaO traced with the rise of fluorescence intensity on microplate reader and fluorescent microscope (Figure 10 and 11) and with the quenching of the fluorescein (Figure 12). Therefore, it was suspected that CaO somehow degraded DMPO or suppressed its ability to bind with oxygen radicals. For a deeper understanding, first, the DMPO solution reacted with CaO and santrifuged. Then the supernatant of the CaO and 0.02 M DMPO suspension was interacted with ZnO under UV light. Since it was known that DMPO-OH spin adduct would form in the presence of ZnO under UV light and ESR signal would be observed, the absence of the characteristic DMPO-OH signal indicated degradation of DMPO. The ESR spectrums of DMPO and CaO interactions were shown on Figure 21.

A clear ESR spectrum of DMPO-OH spin adduct was observed after ZnO-DMPO interaction under UV light (Figure 21(D)). On the other hand, no signal was recorded at ESR measurement of under UV light interaction between ZnO-DMPO that was pretreated with CaO, at the same conditions (Figure 21(B)).

Finkelstein *et al.* [49] reported that hydroxyl and superoxide trapping performance of DMPO decreased with increasing pH values. Therefore, the role of pH on the fading of the ESR signals due to CaO (pH value of CaO suspension was 12.6) was also investigated. Though, signal intensities decreased in a parallel line with Finkelstein *et al.* [49], oxygen radical generation was detected at the ESR measurement of under UV light ZnO interaction with DMPO solution at pH 12.6 (Figure 21(C)). These results indicated that CaO presence damage the structure of DMPO and prevent to fulfil its function. Considering DCFH-DA and fluorescein results, it was thought that, CaO degraded DMPO due to the oxygen radical generation or catalytic reactions.

FT-IR Studies of Coated Samples

In this study, FT-IR analysis was applied to investigate the changes on chemical structure of the coating polymer due to the metal oxide addition. Absorbance spectrums of CaO and ZnO containing PVC coatings were given at Figure 22 and Figure 23, respectively.

FT-IR spectrum of PVC coating (control) which did not contain metal oxide was consistent with former studies [50-52]. C-H stretching around 2916 cm^{-1}, C=O stretching around 1721 cm^{-1}, C-Cl stretching at 833 cm^{-1}, CH rocking at 1272 cm^{-1}, cis-CH wagging around 611 cm^{-1}, CH out of plane bending at 743 cm^{-1} were determined [50-52]. The peak at 3641 cm^{-1} on the Figure 22 originated from CaO existence on the surface [53], the intensity was increased with the increased CaO concentration. Inflexion and stiffening problems were occurred over 20 % CaO addition.

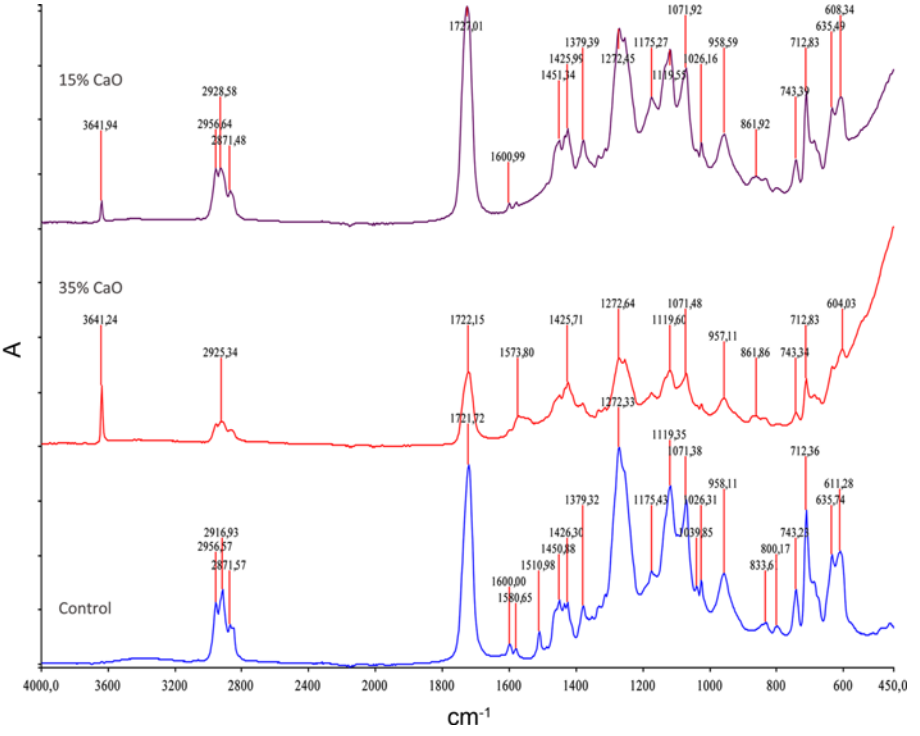

Figure 22. FT-IR spectrums of CaO containing PVC coatings.

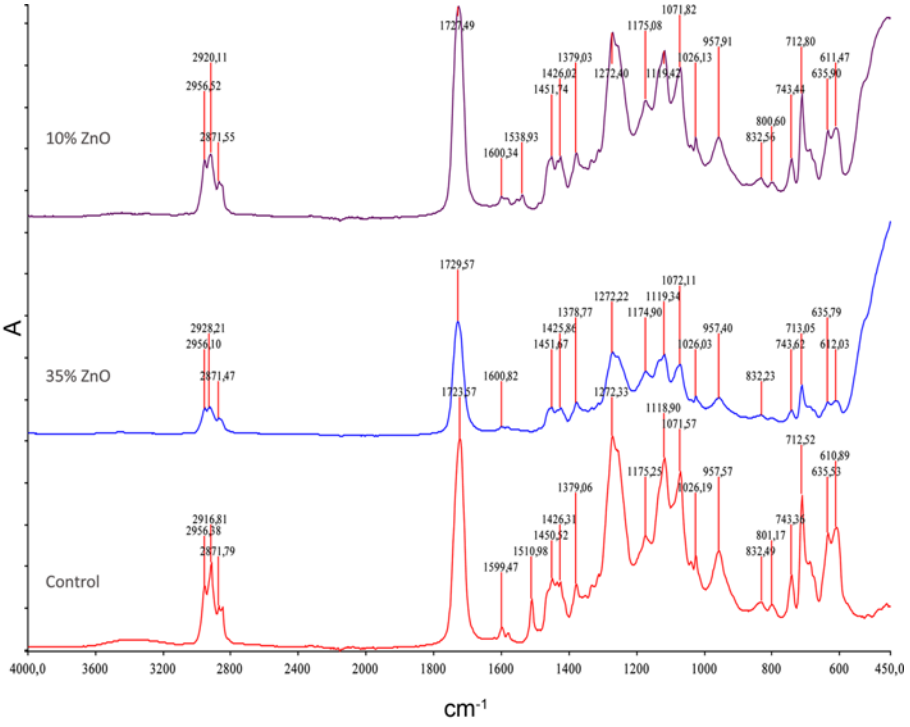

Figure 23. FT-IR spectrums of ZnO containing PVC coatings.

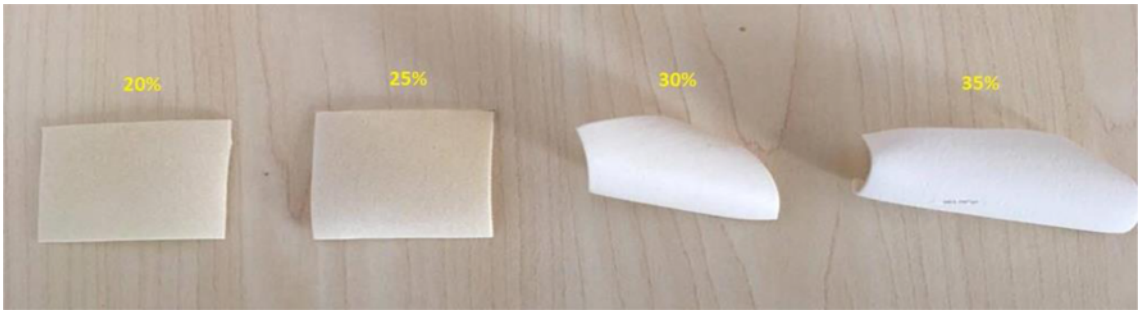

Figure 24. The deformations of CaO containing coated samples.

The deformations of CaO containing coated samples were presented on Figure 24.

Each monomer on the PVC polymer chain contains polar carbon-chlorine bond. Owing to this structural feature, polar parts of plasticizers such as aromatic rings or phthalate esters can bind to polymer with Van der Waals forces or dipol-dipol interactions [54]. Tabb and Koening [52] and Silva *et al.* [51] reported that the peak around 1730 cm^{-1} had been relevant with C=O bond of plasticizer. Experimental studies exhibited that peak area observed around 1730 cm^{-1} was increased with higher plasticizer concentration [51,52]. If Figure 22 is checked, the intensity of the peak around 1730 cm^{-1} was decreased with increased CaO concentration. The dramatic difference between control sample and 35 % CaO containing sample was clearly visible. On this basis, it was thought that CaO addition masked the effect of plasticizer and resulted in stiffness on the second layer of coating led to the inflection of the coated sample. The decreases on the peak intensities of ZnO containing samples were not as sharp as CaO containing samples. Moreover, there was no inflection observed on the ZnO containing samples.

Conclusion

The main scope of this study was to develop metal oxide containing antibacterial polymeric textile coatings especially for conveyor belt materials and to investigate the antibacterial mechanism. Two layered coating system was carried out. The second layer was the functional layer that contains high concentration of metal oxide powder. By this way, either

high antibacterial efficiencies were attained or mechanical properties were preserved. 100 % antibacterial activity detected for 15 % and above concentrations of CaO, 99.9 % antibacterial activity detected for 35 % ZnO concentration and 99.9 % antibacterial activity detected for all investigated concentrations (5-25 %) of MgO. CaO was the most successful additive in terms of antibacterial activity with 100 % bacterial reduction, however, above 20 % CaO concentrations were not recommended due to the inflection problem which was originated from the masking of plasticizer's function by CaO.

Intercellular oxidative stress caused by MgO, ZnO and CaO was detected by DCFH-DA assay by using fluorimetric methods in microplate reader and fluorescent microscope. The highest fluorescent intensity was observed for CaO among the microplate reader test results. Also, CaO and ZnO resulted in quenching of fluorescein in the dark and under UV light, respectively. Fluorescein tests indicated a possible oxygen radical generation or direct catalytic activity. Oxygen radical generation and released oxygen radical amount were determined on ZnO powders and ZnO containing samples by ESR technique using DMPO spin trapping method. The oxidation of DMPO by MgO was detected which is an important clue for oxygen radical generation. No ESR signal was detected from the interaction of DMPO and CaO. The subsequent experiments revealed that DMPO's ability of binding to oxygen radicals disappeared after CaO interaction. Considering DCFH-DA and fluorescein results, it was thought that, high oxygen radical generation or catalytic activity of CaO damaged chemical structure of DMPO. These results are important to understand spin trapping behavior of CaO and MgO with DMPO in ESR technique, since there is no adequate information available in the literature about this issue.

Acknowledgement

This study was funded by Ministry of Science, Industry and Technology of Turkey with the project number: 00883.STZ.2011-1. This study was funded by Dokuz Eylul University Department of Scientific Research Projects with the project number: 2015.KB.FEN.33. The authors would like to thank Rultrans Transmisyon A.S. Kemalpasa/Izmir for their contributions. Antibacterial tests were performed at Izmir Institute of Technology, BIYOMER center. Some of the data in this study was partly presented at following scientific conferences: ICAR 2016 Malaga/Spain, Innovative Solutions for Sustainable Development of Textiles and Leather Industry 2017 Oradea/Romania, UCTEK 2017 Adana/Turkey.

References

1. O. Heide, *Trends Food Sci. Technol.,* **18**, 89 (2007).
2. F. Perez-Rodrıguez, A. Valero, E. Carrasco, R. M. Garcia, and G. Zurera, *Trends Food Sci. Technol.*, **19**, 131 (2008).
3. N. Cioffi and M. Rai, "Nano-Antimicrobials", London, England, 2012.
4. A. Annath, S. Dharaneedharan, H. Seo, M. Heo, and J. Boo, *Chem. Eng. J.,* **322**, 742 (2017).
5. T. O. Okyay, R. K. Bala, H. N. Nguyen, R. Atalay, and Y. Bayam, *RSC Adv.,* **5**, 2568 (2015).
6. V. B. Schwartz, F. Thetiot, S. Ritz, S. Pütz, L. Choritz, A. Lappas, R. Förch, K. Landfester, and U. Jonas, *Adv. Funct. Mater.,* **22**, 2376 (2012).
7. M. Jaissai, S. Baruah, and J. Dutta, *Beilstein J. Nanotechnol*., **3**, 684 (2012).
8. M. Li, L. Zhu, and D. Lin, *Environ. Sci. Technol*., **45**, 1977 (2011).
9. A. Sirelkhatim, S. Mahmud, A. Seeni, N. H. M. Kaus, L. C. Ann, S. K. M. Bakhori, H. Hasan, and D. Mohamad, *Nano -Micro Lett.,* **7**, 219 (2015).
10. J. Sawai, H. Igarashi, A. Hashimoto, T. Kokugan, and M. Shimizu, *J. Chem. Eng. Jpn.,* **28**, 288 (1995).
11. Y. Xie, Y. He, P. L. Irwin T. Jin, and X. Shi, *Appl. Environ. Microbiol.,* **77**, 2325 (2011).
12. O. Yamamoto, *Int. J. Inorg. Mater.,* **3**, 643 (2001).
13. L. Zhang, Y. Jiang, Y. Ding, N. Daskalakis, L. Jeuken, M. Povey, A. J. O'Neil, and D. W. York, *J. Nanopart Res.,* **12**, 1625 (2010).
14. J. M. Yousef and E. N. Danial, *J. Health Sci.,* **2**, 38 (2012).
15. K. Hirota, M. Sugimoto, M. Kato, K. Tsukagoshi, T. Tanigawa, and H. Sugimoto, *Ceram. Int.,* **36**, 497 (2010).
16. L. Huang, D. Li, Y. Lin, D. G. Evans, and X. Duan, *J. Inorg. Biochem*., **99**, 986 (2005).
17. M. Fiedot, I. Maliszewska, O. Rac-Rumijowska, P. Suchorska-Wozniak, A. Lewinska, and H. Teterycz, *Materials*, **10**, 353 (2017).
18. X. Xu, D. Chen, Z. Yi, M. Jiang, L. Wang, Z. Zhou, X. Fan, Y. Wang, and D. Hui, *Langmuir*, **29**, 5573 (2013).
19. V. L. Prasanna and R. Vijayaraghavan, *Langmuir*, **31**, 9155 (2015).
20. D. Wang, L. Zhao, H. Ma, H. Zhang, and L. Guo, *Environ. Sci. Technol*., **51**, 10137 (2017).
21. Farouk, A. Moussa, S. Ulbricht, M. Schollmeyer, and E. Textor, *Text. Res. J.*, **84**, 40 (2014).
22. J. Sawai, E. Kawada, F. Kanou, H. Igarashi, A. Hashimoto, T. Kokugan, and M. Shimizu, *J. Chem. Eng. Jpn.,* **29**, 627 (1996).
23. J. Sawai, H. Kajima, A. Hashimoto, S. Shoji, T. Sawaki, and A. Hakoda, *World J. Microbiol. Biotechnol.,* **16**, 187 (2000).
24. A. Roy and S. S. Gauri, *J. Biomed. Nanotechnol.,* **9**, 1 (2013).
25. S. Makhluf, R. Dror, Y. Nitzan, Y. Abramovic, R. Jelinek, and A. Gedanken, *Adv. Funct. Mater*., **15**, 1708 (2005).
26. J. Sawai, *J. Microbiol. Methods*, **54**, 177 (2003).
27. K. R. Raghupati, R. T. Koodali, and A. C. Manna,

Langmuir, **27**, 4020 (2011).
28. A. Roy, S. S. Gauri, M. Bhattacharya, and J. Bhattacharya, *J. Biomed. Nanotechnol.,* **9**, 1 (2013).
29. Y. Xu and M. A. A. Schoonen, *Am. Mineral.,* **85**, 543 (2000).
30. Y. Li, W. Zhang, J. Niu, and Y. Chen, *ACS Nano*, **6**, 5164 (2012).
31. W. He, Y. Liu, W. G. Wamer, and J. Yin, *J. Food Drug Anal.,* **22**, 49 (2014).
32. V. Roubaud, S. Sankarapandi, P. Kuppusamy, P. Tordo, and J. L. Zweier, *Anal. Biochem.,* **247**, 404 (1997).
33. A. Samouilov, V. Roubaud, P. Kuppusamy, and J. L. Zweier, *Anal. Biochem.* **334**, 145 (2004).
34. A. Aranda, L. Sequedo, L. Tolosa, G. Quintas, E. Burello, J. V. Castell, and L. Gombau, *Toxicol. in Vitro,* **27**, 954 (2013).
35. D. Armstrong, "Advanced Protocols in Oxidative Stress II", New York, USA, 2010.
36. R. P. Rastogi, S. P. Singh, D. Hader, and R. P. Sinha, *Biochem. Biophys. Res. Commun.,* **397**, 603 (2010).
37. J. Hua, M. Shao, L. Cheng, X. Wang, Y. Fu, and D. D. D. Ma, *J. Phys. Chem. Solids*, **70**, 192 (2009).
38. M. Bardhan, G. Mandal, and T. Ganguly, *J. Nanosci. Nanotechnol.,* **11**, 3418 (2011).
39. E. C. Friedly, MS Thesis, University of Arkansas. Arkansas, USA, 2007.
40. B. Mizrak, Personal Contact. Rultrans Transmisyon A. S. Kemalpasa/İzmir-Turkey, 2016.
41. A. Lipovsky, Z. Tzitrinovich, H. Friedmann, G. Applerot, A. G. Lubart, and R. Lubart, *J. Phys. Chem. C,* **113**, 15997 (2009).
42. G. Applerot, A. Lipovsky, R. Dror, N. Perkas, Y. Nitzan, R. Lubart, and A. Gedanken, *Adv. Funct. Mater.,* **19**, 842 (2009).
43. S. L. Baum, I. G. M. Anderson, R. R. Baker, D. M. Murphy, and C. C. Rowlands, *Anal. Chim. Acta,* **481**, 1 (2003)
44. UK Standards for Microbiology Investigations - Identification of *Listeria* Species, and other Non-sporing Gram Positive Rods (except *Corynebacterium*). Public Health England. Bacteriology – Identification, ID 3, Issue no: 3. 1, Issue date: 29. 10. 2014.
45. M. Kurth, P. C. J. Graat, H. D. Carstanjen, and E. J. Mittemeijer, *Surf. Interface Anal.,* **38**, 931 (2006).
46. E. Finkelstein, G. M. Rosen, and E. J. Rauckman, *J. Am. Chem. Soc.,* **102**, 4994 (1980).
47. S. Ramesh, K. H. Leen, K. Kumutha, and A. K. Arof, *Spectrochim. Acta, Part A,* **66**, 1237 (2007).
48. M. A. Silva, M. G. A. Vieria, A. C. G. Maçumoto, and M. M. Beppu, *Polym. Test.,* **30**, 478 (2011).
49. D. L. Tabb and J. L. Koenig, *Macromolecules*, **8**, 929 (1975).
50. S. Nasrazadani and E. Eureste, "Application of FTIR for Quantitative Lime Analysis", 5-9028-01 Project Report University of North Texas. Texas, USA, 2008.
51. P. H. Daniels, *J. Vinyl Add. Tech.,* **15**, 219 (2009).